International Journal of Applied Earth Observation and Geoinformation 132 (2024) 103994

Contents lists available at ScienceDirect

International Journal of Applied Earth Observation and Geoinformation

journal homepage: www.elsevier.com/locate/jag

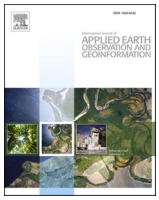

ALOS-2 PALSAR-2 ScanSAR and Sentinel-1 data for timely tropical forest disturbance mapping: A case study for Sumatra, Indonesia

Johannes Balling [a,*], Bart Slagter [a], Sietse van der Woude [a], Martin Herold [a,b], Johannes Reiche [a]

[a] Wageningen University, Laboratory of Geo-Information Science and Remote Sensing, Wageningen, the Netherlands
[b] Helmholtz GFZ German Research Centre for Geosciences, Remote Sensing and Geoinformatics, Potsdam, Germany

ARTICLE INFO

Keywords:
Tropical forest
Forest disturbance
SAR
ALOS-2 ScanSAR
Sentinel-1
C-Band
L-Band

ABSTRACT

Precise and prompt information on forest disturbances in the tropics is critical to support law enforcement and protect tropical forests. In 2023, medium resolution ALOS-2 ScanSAR data (~100 m spatial resolution) was made available for Southeast Asia, marking the first freely accessible large-area L-Band dataset. We assessed its potential for large-area forest disturbance mapping and its combination with high-resolution C-band Sentinel-1 data (~20 m spatial resolution). We mapped forest disturbances in Sumatra, Indonesia for the year 2021 based on ALOS-2 ScanSAR data and Sentinel-1 data separately, and subsequently combined the mapped disturbances. Forest disturbances detected by both C-band and L-band SAR using a probabilistic change algorithm were combined at the product level by merging both sets of detections. The added benefit of combining both sensors was particularly evident in higher detection rates, as indicated by an improved producer accuracy (78.9 ± 11.9 %) compared to detections based on single sensor ALOS-2 ScanSAR (40.8 ± 6.3 %) and Sentinel-1 data (63.3 ± 9.6 %). Both combined and single sensor detections showed negligible false detections. ALOS-2 ScanSAR showed advantages for overcoming limited capability of Sentinel-1 to detect large-sized disturbance events characterized by post-disturbance tree remnants, occurring at locations with large-scale agricultural clearings. The medium resolution of approximately 100 m restricts the detection capability of ALOS-2 ScanSAR data for small-scale disturbances, resulting in missed detections. ALOS-2 ScanSAR detections showed a delay of up to 17.8 days compared to detections based solely on Sentinel-1 data. Combining ALOS-2 ScanSAR and Sentinel-1-based disturbances resulted in improved detection timeliness, with an average improvement of up to 16.5 days compared to Sentinel-1-based detections. Furthermore, we observed improved detection rates for our ALOS-2 ScanSAR-based detections compared to those of the ALOS-2 ScanSAR-based *JICA-JAXA Forest Early Warning System in the Tropics* (JJ-FAST) forest disturbance alerting product. This suggests that the potential of ALOS-2 ScanSAR data in operational forest monitoring systems is not currently fully realized. Comparing the SAR-based disturbance detections from this study with existing optical-based forest disturbance products (GFC and GLAD-L) suggested improved detection accuracies by overcoming sensor-specific omission errors when using combined SAR and optical data. The demonstrated potential of L-Band ALOS-2 ScanSAR data for improving operational forest monitoring efforts using C-band radar and optical satellites is expected to be amplified by upcoming L-Band satellite missions like NiSAR (2024) and ROSE-L (2028), which will provide freely accessible L-Band data with higher spatial resolution.

1. Introduction

Forests in the tropics are vital for the global carbon cycle and biodiversity (Boulton et al., 2022; Sullivan et al., 2017). However, in recent years, increasing levels of forest disturbances pose a threat to tropical forests (Vancutsem et al., 2021). Indonesia is among the countries experiencing some of the highest rates of deforestation worldwide (Margono et al., 2014), primarily driven by agricultural expansion, timber production and mining, with fires frequently employed as a means of land clearing in management practices (Abood et al., 2015; Gaveau et al., 2014; Sloan et al., 2017). Detecting forest disturbances in a timely and accurate manner is crucial to support law enforcement activities, which ensures sustainable land management practices and protects remaining tropical forests (Finer et al., 2018; Tabor and

* Corresponding author.
E-mail address: johannes.balling@wur.nl (J. Balling).

https://doi.org/10.1016/j.jag.2024.103994
Received 11 March 2024; Received in revised form 24 May 2024; Accepted 22 June 2024
Available online 7 July 2024

Holland, 2021).

Remote sensing has demonstrated its usefulness as an affordable tool to monitor tropical forest and detect tropical forest disturbances at scale (De Sy et al., 2012). Optical sensors, including Landsat and Sentinel-2, have been used to track forests and detect forest disturbances, commonly by means of spectral vegetation indices (Chen et al., 2021; Hamunyela et al., 2016; Verbesselt et al., 2012). In tropical regions, optical sensors may suffer from persistent cloud coverage resulting in delayed or missed detections when monitoring forest disturbances (Doblas Prieto et al., 2023; Hirschmugl et al., 2020). In contrast, Synthetic Aperture Radar (SAR) sensors actively emit radar signals that are capable of penetrating clouds (Joshi et al., 2016). The radar signal is sensitive to the vegetation structure and moisture content (Richards, 2009; Woodhouse, 2006). The radar signal interacts with the vegetation structure depending on its polarization and wavelength and the size, spatial orientation, and density of the vegetation structure components (Flores-Anderson et al., 2019). The backscatter of the signal emitted in horizontal or vertical polarizations can be received in co-polarization (e.g., HH or VV) or cross-polarization (e.g., HV or VH). The recorded backscatter intensity received in various polarizations relates to the spatial orientation and density of the sensed objects (Woodhouse, 2006). The wavelength of the radar signal determines the size of object that it can penetrate or interact with. Shorter wavelengths, like those in C-Band, interact with smaller objects, while longer wavelengths, such as L-Band, penetrate smaller objects and interact with larger ones (Ulaby and Long, 2013). In tropical broadleaf forest, C-Band radar will interact with twigs and leaves, while L-Band radar can penetrate parts of the canopy and interact with branches or tree trunks. L-Band is considered better suited for detecting tropical forest disturbances due to its greater depth of penetration and increased saturation level (Reiche et al., 2018; Ulaby and Long, 2013; Woodhouse, 2006). Current large-scale tropical forest disturbance systems, such as *RAdar for Detecting Deforestation* (RADD) (Reiche et al., 2021) or *Near-Real Time System for Detection of Deforestation* (DETER-R) (Doblas et al., 2022), primarily rely on freely available Sentinel-1 C-Band SAR data (Ballère et al., 2021; Mermoz et al., 2021), despite of C-Band being demonstrated as less suitable for detecting tropical forest disturbances.

Tropical forest disturbance monitoring based on high-spatial resolution ALOS-2 PALSAR-2 Fine Beam data has showcased the capabilities of L-Band SAR data (Ali et al., 2018; Reiche et al., 2018). However, the low temporal resolution of 46 days and limited free data access hamper large-scale applications. ALOS-2 PALSAR-2 ScanSAR data holds great potential for promptly detecting forest disturbances due to its wide swath and resulting rapid revisit time of 14 days, despite having a medium spatial resolution of approximately 100 m (Table 1). So far, the usage of ALOS-2 ScanSAR data was focused primarily to height estimation of tropical forests (Urbazaev et al., 2018) and SAR interferometry applications, such as studying the impact of earthquakes (Liang and Fielding, 2017; Natsuaki et al., 2016). Studies demonstrating the potential of ScanSAR data for disturbance detection did not incorporate ALOS-2 data, which offers an improved temporal resolution of up to 14 days, but instead relied on ALOS-1 data with a temporal resolution of 46 days (Valeriano and Amaral, 2010; Whittle et al., 2012).

The operational forest disturbance alerting system *JICA-JAXA Forest Early Warning System in the Tropics* (JJ-FAST) produced internally by the *Japan International Cooperation Agency* (JICA) and the *Japan Aerospace Exploration Agency* (JAXA) is based on ALOS-2 ScanSAR data (Watanabe et al., 2021, 2018). A minimum mapping unit of 1 ha limits the system to detect large-sized disturbance events only and potentially neglects the potential of ALOS-2 ScanSAR data (Watanabe et al., 2021, 2018). In 2023, ALOS-2 ScanSAR level 2.2 data became freely available for Southeast Asia. This is the first time L-Band data is openly accessible for large areas, enabling the assessment of the large-scale potential of L-Band SAR data for forest disturbance detections. These insights can contribute to an improved comprehension of the constraints and capabilities of L-Band SAR data in supporting large-scale forest disturbance detection. This becomes particularly relevant in preparation for upcoming satellite missions like NiSAR and ROSE-L, which will provide freely available L-Band SAR data (Table 1). These data streams will provide further opportunities to combine freely available L-Band SAR data with Sentinel-1 (C-Band) SAR data for tropical forest monitoring at scale.

In this study, we assess the potential of medium resolution ALOS-2 ScanSAR data (L-Band) for large-scale tropical forest disturbance mapping and evaluate its effectiveness when combined with high-resolution Sentinel-1 data (C-Band).

In a case study conducted in Sumatra (Indonesia), we first detect forest disturbances based on ALOS-2 ScanSAR and Sentinel-1 data separately for 2021. Subsequently, we combine both single-sensor detections. We calculated the detection accuracies, mapped area statistics and detection timeliness of the individual single-sensor detection and combined detections, to assess the strengths, limitations, and combined potential of both datasets to detect forest disturbances. Additionally, we compare ALOS-2 ScanSAR-based forest disturbance detections of this study with detections of the JJ-FAST alerting system to better understand the potential of ALOS-2 ScanSAR data. *Similarly, we* assessed the benefits of SAR-based forest disturbance detections in relation to optical-based disturbance detections by comparing SAR-based disturbance detections of this study against disturbances identified by the Landsat-based GLAD-L alerting system (Hansen et al., 2016) and the annual GFC (Global forest change) product (Hansen et al., 2013).

2. Study area and data

2.1. Study area

The study area includes the main island of Sumatra (Indonesia) and its smaller adjacent islands, comprising an area of approximately 47.500 kha (Fig. 1). Sumatra experiences a tropical humid climate with elevated temperatures and high precipitation persisting throughout the year

Table 1
Current and upcoming SAR satellite missions operating at L-Band wavelength.

Mission	Start(End of expected Lifetime)	Agency	Spatial Resolution [m]	Revisit time [days]	Data policy	Reference
ALOS – 2 PALSAR – 2	2014 (2019)	JAXA	Stripmap mode:3– 10 ScanSAR mode: 60 – 100	14	Mainly Commercial	(JAXA, n.d.)
SAOCOM	2018 (1A: 2023 &1B: 2025)	CONAE	Stripmap mode: 10 TopSAR mode: 30 – 100	8 (16)	Freely available	(ESA, n.d.)
NiSAR	Planned for 2024(2029)	NASA & ISRO	3 – 10 m	12	Freely available	(NASA, n.d.)
ALOS – 4 PALSAR – 3	Planned for 2024(2031)	JAXA	Stripmap mode:3 – 10 ScanSAR mode:25 (1 look)	14	Commercial	(Motohka et al., 2019)
ROSE-L	Planned for 2028 (A: 2035B: 2037)	ESA	5 – 50 m	6 (12)	Freely available	(ESA, 2023)

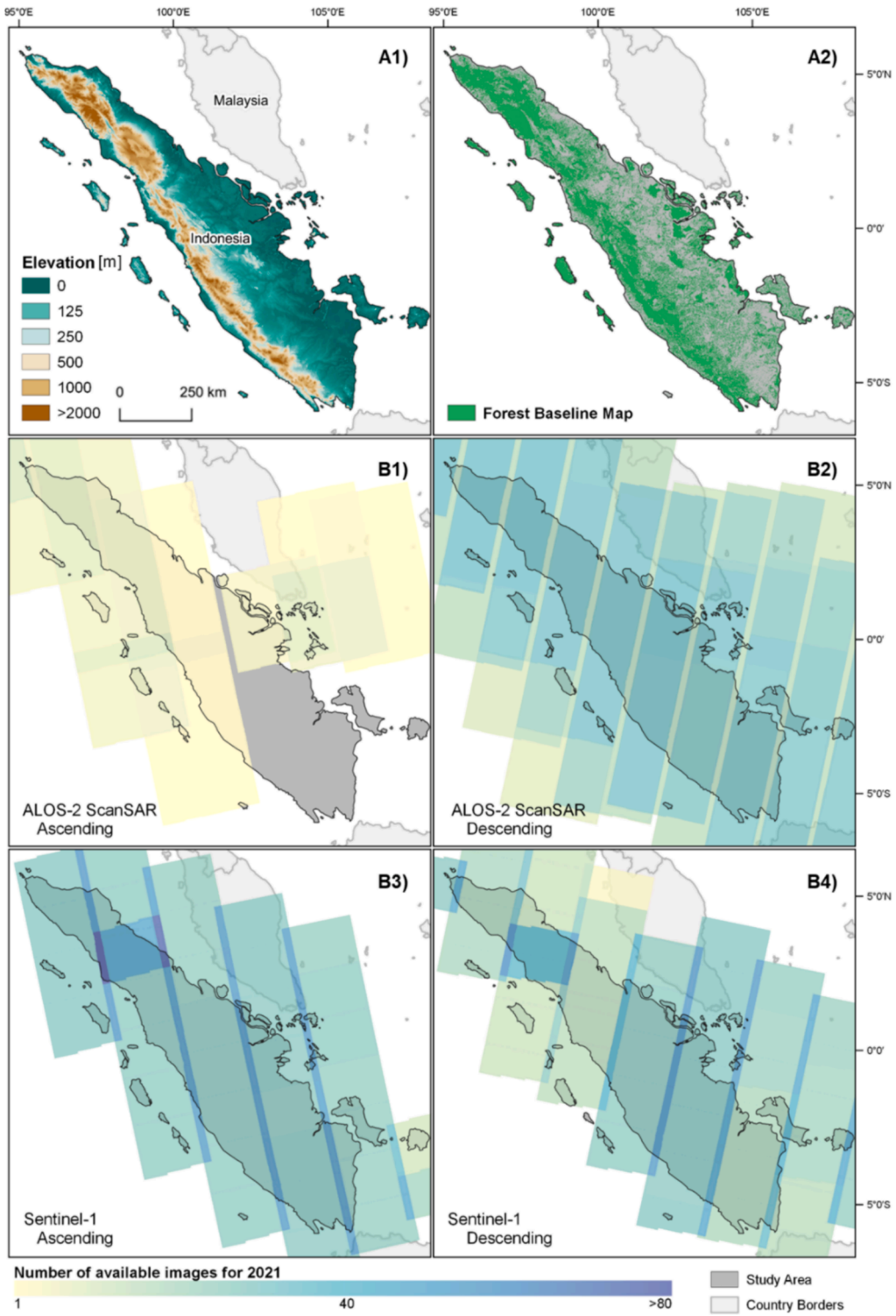

Fig. 1. Study Area of Sumatra (Indonesia). Elevation (A1) and the extent of the used forest baseline map (A2) are provided. Additionally shown are the number of available images for ALOS-2 ScanSAR (ascending: B1; descending: B2) and Sentinel-1 data (ascending: B3 and descending: B4) for 2021.

(Hayasaka, 2023). The main island of Sumatra consists of two very distinct parts: the Barisan Mountains in the west, featuring elevations exceeding 2000 m, and flat plains in the east (Fig. 1A1). The flat plains in particular have experienced high deforestation rates, resulting in the conversion of 70 % of primary forest to other land cover by 2010 (Margono et al., 2012). Deforestation activities are primarily driven by commercial agriculture crop expansion and timber extraction (Austin et al., 2019; Margono et al., 2014). Disturbance activities occur throughout Sumatra with distinct proximity to areas of high human footprints (Singh and Yan, 2021). Sumatra is predicted to experience continuous forest loss in the future, making it a prime region to study the potential of medium resolution ALOS-2 ScanSAR (L-Band) for tropical forest disturbance mapping (Abood et al., 2015; Saputra and Lee, 2019).

2.2. Data

2.2.1. ALOS-2 PALSAR-2 ScanSAR data

ALOS-2 PALSAR-2 Level 2.2 ScanSAR normalized L-Band backscatter data acquired in broad area observation mode was used. The data is provided in dual-polarization (HH- and HV-polarization). ALOS PALSAR-2 ScanSAR data in ascending and descending orbits for the period 2017–2021 were accessed via Google Earth Engine. The data is provided at a pixel spacing of 25 × 25m, although the spatial resolution is approximately 100 m (JAXA, 2023). Although there is a potential revisit time of 14 days, we observed almost no observations in ascending orbit and 18–36 observations in descending orbit for the year 2021 (Fig. 1B1, B2).

2.2.2. Sentinel-1 data

Sentinel-1 A/B Interferometric Wide swath C-Band data was used. Here, Ground Range Detected (GRD) data was available in VV- and VH-polarization. Ascending and descending orbits covering the years 2017–2021 were accessed through Google Earth Engine. The data is provided at a pixel spacing of 10x10m, although the spatial resolution is approximately 20 m (ESA, 2012). The revisit time of two Sentinel-1 satellites in the tropics is up to 6 days (ESA, 2022). We observed 30–84 observations in ascending and 16–60 observations in descending orbits for the year 2021 (Fig. 1B3, B4).

2.2.3. JJ-FAST product

JJ-FAST is a forest disturbance alerting product providing information on disturbances for the pan-tropics, including 78 countries (Watanabe et al., 2021, 2018). JJ-FAST detections have a pixel spacing of 50x50m and are based on dual-polarization ALOS-2 PALSAR-2 ScanSAR data (JICA and JAXA, 2023a). The spatial resolution of the underlying L-Band data is approximately 100 m. The product's minimum mapping unit is currently 1 ha (Version 4.1), with older versions showing coarser minimum mapping units (1.5 for version 4.0-3.1 and 2 ha for version 3.0) (JICA and JAXA, 2024). Detections utilizing version 3.1 or subsequent versions are created based on a forest baseline map that is directly derived from the individual ALOS-2 ScanSAR images (JICA and JAXA, 2023a). Older versions used the global ALOS PASLAR forest/non-forest product as the underlying forest baseline map. All JJ-FAST detections available for 2021 (Version 3.0) were accessed and downloaded through JJ-FAST's MapMonitor (JICA and JAXA, 2023).

2.2.4. Landsat-based forest disturbance products

The GFC product and the GLAD-L product provide forest disturbance information at a 30 m spatial resolution and are based on optical Landsat data. Both products are produced by the University of Maryland. The GFC, introduced in 2013, is a global forest change product providing annual information on forest disturbances (Hansen et al., 2013). In contrast, GLAD-L is an alerting system that provides information on forest disturbances in near real time for the entire pantropics (30°N-30°S) from 2016 onwards (Hansen et al., 2016).

2.2.5. Forest baseline map

We created a forest baseline map for 2021 (Fig. 1A2) using a Global Forest Change product based on Landsat-data (Hansen et al., 2013). We defined forest as tree cover exceeding 30 % for the year 2000 and removed forest disturbances occurring between 2001 and 2020 prior to the study's monitoring period in 2021. Our forest baseline map covers approximately 27,000 kha.

3. Methods

3.1. Pre-processing of SAR data

Both ALOS-2 ScanSAR and Sentinel-1 GRD data are provided with initial pre-processing steps applied before their ingestion into Google Earth Engine. The ALOS-2 ScanSAR data has been ortho-rectified and radiometrically terrain-corrected using the AW3D30 Digital Surface Model providing γ0 backscatter (Small, 2011). The Sentinel-1 data has undergone radiometric and terrain correction, among other processes, and has been geocoded (Google Earth Engine Team, 2022).

We further applied additional pre-processing steps to both datasets (Table 2) (Mullissa et al., 2021). In order to obtain γ0 backscatter for the Sentinel-1 GRD data we applied an angular-based radiometric slope correction (Hoekman and Reiche, 2015; Vollrath et al., 2020). The correction was not applied to ALOS-2 ScanSAR data, as this data is initially provided as fully terrain-corrected γ0 backscatter. We masked terrain artifacts in the ALOS-2 ScanSAR data using the provided quality band with an additional buffer of 100 m (native resolution of the data) to ensure no remaining artifacts (JAXA, 2023; Small, 2011).

An adaptive multi-temporal speckle filtering was applied to both ALOS-2 ScanSAR and Sentinel-1 data, before converting the data to dB scale (Quegan and Yu, 2001).

Sentinel-1 data acquired in Interferometric Wide swath mode have small overlapping areas at the image edges in the range direction (Fig. 1B3, B4), leading to areas with large differences in incidence angles between orbits. We only considered observations from the most frequent orbit between 2017 and 2020 in order to avoid combining large differences in incidence angles, which could introduce errors in disturbance detections (Reiche et al., 2021). ALOS-2 ScanSAR data acquired in broad area observation mode does not show overlapping areas of image edges with large differences in incidence angle and therefore did not require corrections (Fig. 1B1, B2).

SAR data can be affected by heavy rain cells causing decreased backscatter and false detections in forest disturbance detection algorithms (Doblas et al., 2020). Rain cells are visible as large patches of connected pixels with decreased backscatter values in SAR observations. Furthermore, rain cells are typically short-lived, resulting in decreased backscatter values for no more than one observation. The impact of rain cells is more pronounced in shortwave SAR data, like C-Band Sentinel-1, whereas longer wavelength radar, such as L-Band ALOS-2 ScanSAR data, can penetrate rain cells more effectively (Danklmayer et al., 2009). Rain cell masking was therefore only applied to Sentinel-1 data. Here, decreased backscatter occurring in large clusters of pixels for only one time step over forest was masked out as an artifact caused by rain cells (Reiche et al., 2021).

We applied image normalization to ALOS-2 ScanSAR and Sentinel-1 data, by normalizing individual images to mitigate potential false detections due to decreased backscatter values during the dry season. We compared the expected historic median backscatter time series value (2017–2020) against the median backscatter values of an observation and – if required – matched the median backscatter distribution (Reiche et al., 2018).

3.2. Forest disturbance mapping

We mapped forest disturbances for 2021 within the boundaries of the forest baseline map (Chapter 2.2.5), using ALOS-2 ScanSAR and Sentinel-1 data separately. We followed the definition of forest disturbance as the partial or complete removal of forest cover within an ALOS-2 ScanSAR (25 m) or a Sentinel-1 (10 m) pixel, in line with recent studies (Balling et al., 2023; Hansen et al., 2016; Reiche et al., 2021; Vargas et al., 2019).

We employed an algorithm for probabilistic change detection on a pixel level (Reiche et al., 2018, 2015), which also provided the basis for generating the RADD alerts (Reiche et al., 2021). SAR time series from 2017 to 2020 were used to compute statistics of backscatter values (mean and standard deviation) for stable forest and to establish parameters for a Gaussian Mixture Model. The utilization of the Gaussian Mixture Model was implemented to compute non-forest probability values for individual new observations. After calculating non-forest probabilities separately for each polarization, the highest probability

Table 2
Prior (o), additional (x) and pre-processing steps not (–) applied to the SAR data used in this study.

	Slope correction	Quality band masking	Speckle filtering	Conversion to dB scale	Dominant orbit masking	Rain cell masking	Image Normalization
ALOS-2 PALSAR-2 ScanSAR Level 2.2	o	x	x	x	–	–	x
Sentinel-1 GRD Level 1	x	–	x	x	x	x	x

of both polarizations was selected and set as the non-forest probability for the respective observation. New observations exceeding a non-forest probability of 60 % were flagged as potential forest disturbances. Within a 90-day period, disturbances in each new observation, which had been flagged and which had a non-forest probability exceeding 97.5 % were confirmed (high-confidence alert), while those with a non-forest probability below 85 % were rejected. Flagged disturbances with a non-forest probability that remained between 85 and 97.5 % were left flagged and unconfirmed (low confidence alert). The date of the disturbance was assigned as the date when it was initially flagged. In wetland areas, co- and cross-polarization were used to flag potential disturbances, while a confirmation relied exclusively on the cross-polarization. This was done to mitigate potential false detections in the co-polarization due to heighten sensitivities toward soil moisture changes and increased double bounce scattering caused by floods (Refice et al., 2020). We used CIFOR's global tropical and subtropical wetlands map to locate wetlands (Gumbricht et al., 2017).

For ALOS-2 ScanSAR data, we detected disturbances as decreasing backscatter values in HV-polarization and as increasing or decreasing backscatter in HH-polarization. Decreasing backscatter in HV-polarization is caused by reduced volume scattering, indicating a loss of forest structure, whereas decreasing HH-polarization is caused by a reduced double bounce scattering, indicating a disruption in the alignment or orientation of the branches or trunks. However, increased backscatter in HH-polarization can be caused by enhanced double bounce on post-disturbance tree remnants (e.g., trunks, branches) (Watanabe et al., 2021). For Sentinel-1, we exclusively detected decreasing backscatter values in both VV- and VH-polarizations, as they are indicative of alterations in volume scattering, double bounce, or surface scattering. These alterations are typically observed during the transition from forest to non-forest areas (Richards, 2009; Woodhouse, 2006). We applied a minimum mapping unit of 0.1 ha. Forest disturbance event sizes were calculated as connected detections on a pixel-level (8-connected).

Combined C- and L-band disturbance detections were generated through post-classification merging at a product level, which involved incorporating both ALOS-2 and Sentinel-1 based detections. In case of overlapping detections, we chose the earliest detection date from either sensor. The pixel spacing used for the combination was 10 m.

3.3. Detection accuracy and evaluation of timeliness

To validate the disturbance detections, we utilized monthly composites of very-high-resolution multi-spectral PlanetScope data (~4.7 m) (Planet Team, 2022). We visually checked for the presence of a forest disturbance. In cases where environmental factors (e.g., clouds, haze, etc.) hampered a visual interpretation of the Planet data (31 samples), we used the original ALOS-2 ScanSAR and Sentinel-1 time series to verify the occurrence of a disturbance (ESA, 2012; JAXA, 2023).

Employing a stratified random sampling method (Olofsson et al., 2014; Stehman et al., 2003), we incorporated two stable forest strata and six disturbance strata. The stable forest strata encompassed all pixels within the forest baseline map, with one stratum sampling outside and the other inside a 500 m buffer surrounding identified forest disturbances. The latter was included to mitigate the potential underrepresentation of omission errors (Olofsson et al., 2020).

The six forest disturbance strata were delineated into two primary disturbance categories: forest disturbance detected by both sensors and forest disturbance detected by only one sensor. Each main disturbance stratum was then divided into three separate strata based on the size of the detected disturbance event: $<$1ha, $\geq$1 – $<$5ha and $\geq$5 ha. The sizes of the disturbance events were calculated individually, based on the combined map of forest disturbance detections from ALOS-2 ScanSAR and Sentinel-1 data.

We introduced the 'detected by only one sensor' disturbance stratum to address potential omission errors and false detections in either of the single disturbance detections. Furthermore, we incorporated the refinement of the two main disturbance strata into event size-based strata to accommodate differing spatial resolutions of ALOS-2 ScanSAR and Sentinel-1 data. In total, we utilized 1000 samples, comprising of 200 samples for each stable forest stratum and 100 samples for each of the forest disturbance strata (Table 3). The combined disturbance map of ALOS-2 ScanSAR and Sentinel-1 data was used to generate the strata and area statistics. As proposed by Stehman et al. (2003), we calculated inclusion probabilities to account for samples not being proportionally allocated to the strata areas. We then used these inclusion probabilities as estimation weights to construct an area-weighted confusion matrix and calculate user and producer accuracies (Stehman, 2014). Errors resulting from an inaccurate forest baseline map, which may suffer from typical errors found in optical remote sensing products (Verhelst et al., 2021), were excluded when calculating the accuracies.

We calculated the differences in the detection dates of ALOS-2 ScanSAR-based and Sentinel-1 based detection to assess the improvement of timeliness. The same method was applied to the combined forest disturbances detection. The improvement or delay in timeliness were calculated relative to the disturbance date detected by Sentinel-1 data. Only disturbances detected by both ALOS-2 ScanSAR and Sentinel-1 data were taken into consideration. Timeliness is defined here as the date when a forest disturbance is detected. Therefore, an enhancement in timeliness refers to detecting disturbances at an earlier date.

3.4. Comparison with JJ-FAST & Landsat-based products

We calculated and compared accuracies of ALOS-2 ScanSAR-based disturbance detections from this study with JJ-FAST detections. Accuracies were calculated using a post-stratification on the validation data set. Here, we only included samples that match the overlap of the forest baseline maps used in this study and applied for the JJ-FAST product (430/1000) and reduced the validation strata accordingly. For the samples in the reduced strata, the inclusion probabilities were recalculated (Tsendbazar et al., 2021), and area-adjusted user and producer accuracies were calculated for the JJ-FAST product and ALOS-2 ScanSAR-based disturbance detections of this study, following the methodology described in Chapter 3.3.

To specifically evaluate errors in small-, medium- and large-sized disturbance events, we additionally examined area-adjusted accuracies for each disturbance event size class alone. Therefore, we combined accuracies of the respective event size strata of forest disturbance detected by both sensors and forest disturbance detected by only one sensor (Chapter 3.3).

For the validation of the Landsat-based forest disturbance alerting system GLAD-L and the annual GFC product we used all initial samples

Table 3
Validation strata and corresponding sample sizes.

Strata	Stable forest (outside buffer)	Stable forest (inside buffer)	Forest disturbance detected by only one sensor Disturbance event size [ha]			Forest disturbance detected by both sensors		
			<1	≥1 –5	≥5	<1	≥1 –5	≥5
Number of Samples	200	200	100	100	100	100	100	100

and the validation procedure described in Chapter 3.3. We calculated user and producer accuracies accordingly. The original samples described in Chapter 3.3 were applicable because our forest baseline map, and therefore our validation strata, were based on the GFC product.

4. Results

4.1. Forest disturbance mapping

High omission rates were observed in single-sensor mapping (Fig. 2). A higher producer accuracy (1 – omission error) was found for Sentinel-1 (63.3 ± 9.6 %) compared to ALOS-2 ScanSAR (40.8 ± 6.3 %). Negligible false detection rates (1 – user accuracy) were found for both ALOS-2 ScanSAR (UA: 98.6 ± 0.8 %) and Sentinel-1 (UA: 100 ± 0 %). Combining mapped forest disturbances from Sentinel-1 and ALOS-2 ScanSAR resulted in reduced omission errors (PA: 78.9 ± 11.9 %), while maintaining a low false detection rate (UA: 99.3 ± 0.4 %).

More forest disturbances were detected based on Sentinel-1 data (379.3 kha) in comparison to ALOS-2 ScanSAR-based detections (291.3 kha) (Table 4). Disturbances detected based on only Sentinel-1 data showed equal proportions for small- (35.6 %), medium- (30.2 %) and large-sized (34.2 %) disturbance events. For ALOS-2 ScanSAR data, we observed a trend of higher detection rates for larger-sized disturbance events. In this context, large-sized disturbance events (≥5ha) accounted for 50.5 %, while medium- (31.1 %) and small-sized (18.4 %) disturbance events showed substantially smaller proportions.

The combined detections showed slightly higher proportions for large-sized events (39.9 %) compared to small- (29.6 %) and medium-sized (30.4 %) disturbance events. Combining ALOS-2 ScanSAR and Sentinel-1 based disturbances detections showed the highest detection rate of 510.8kha, indicating an increase of 219.5 kha and 131.5 kha in detections compared to ALOS-2 ScanSAR and Sentinel-1 disturbances maps, respectively.

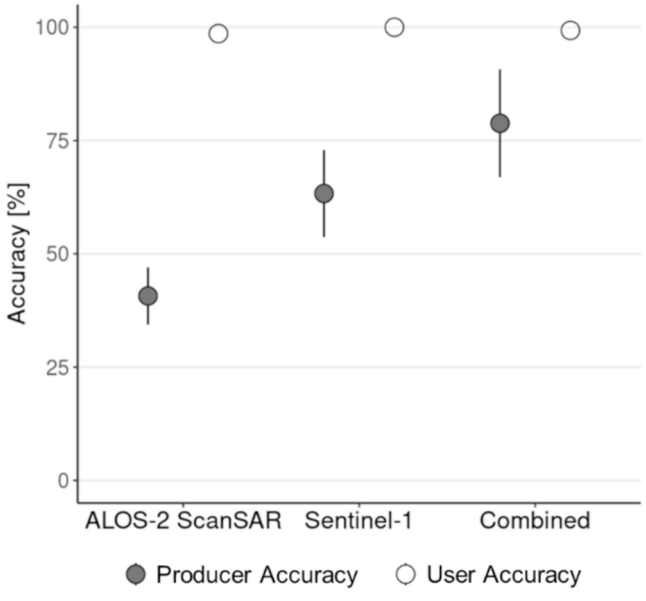

Fig. 2. Producer and user accuracies (±standard error) for disturbances detected based on ALOS-2 ScanSAR (L-Band) and Sentinel-1 data (C-Band) and the combined detections.

When compared to Sentinel-1 based detections, we observed higher omission rates in ALOS-2 ScanSAR-based detections for small-scale disturbances, such as selective logging or logging roads (Fig. 3a). Logging roads were typically partially detected by Sentinel-1 but entirely omitted by ALOS-2 ScanSAR. The combined forest disturbance detections primarily consisted of Sentinel-1 detections in these regions.

For medium-sized disturbance events, we observed omission errors for ALOS-2 ScanSAR and Sentinel-1 based detections (Fig. 3b). Omission errors in ALOS-2 ScanSAR disturbance detections occurred for disturbances within the forest but in spatial proximity to roads (e.g., selective logging, timber extraction, etc.). The Sentinel-1 disturbance detections showed omission errors for disturbance patches characterized by post-disturbance tree remnants. The combined detections did not show either of the omission errors.

For large-sized disturbance events, such as large-scale clearings associated with agricultural expansion or timber production, we observed the benefit of ALOS-2 ScanSAR-based detections, showing fewer omission errors in areas with post-disturbance tree remnants (Fig. 3c). However, omission errors were noticeable in ALOS-2 ScanSAR detections, typically in the case of small, isolated forest patches that had been detected using Sentinel-1 data (Northwest in Fig. 3c).

4.2. Detection timeliness

Forest disturbances detected with ALOS-2 ScanSAR showed an average detection delay of 18 days when compared to those detected with Sentinel-1 (Table 5). A decreasing detection delay was observed for increasing forest disturbance event sizes. While small-sized disturbance events showed a 21-day average detection delay, a 12-day detection delay was observed for large-sized events. Timeliness improved when combining forest disturbances detected with ALOS-2 ScanSAR and Sentinel-1 data. New disturbances were detected, on average, 16.5 days earlier compared to detections based on Sentinel-1 data alone. Overall, improvement rates were consistent across small-, medium- and large-sized disturbance events.

4.3. Comparison with JJ-FAST & Landsat-based products

Disturbances detected based on ALOS-2 ScanSAR in this study (producer accuracy: 55.8 ± 6 %) showed substantially lower omission rates than the JJ-FAST product (producer accuracy: 29.2 ± 4.1 %) (Fig. 4). Low false detection rates were observed for both. We observed increasing producer accuracies for larger disturbance event sizes. ALOS-2 ScanSAR-based detections in this study showed consistently higher producer accuracies than JJ-FAST detections. Particularly, for medium-sized events, there was a notable 43.6 % difference between the two detections, with a higher producer accuracy for detections in this study (57 ± 4.1 %) compared to the JJ-FAST product (13.4 ± 3.4 %). The same was evident when exclusively considering flatlands (≤5°), with ALOS-2 ScanSAR detections in this study showing a higher producer accuracy (59.6 ± 6.4 %) than the JJ-FAST product (33.3 ± 5 %). Applying coarser minimum mapping units, corresponding to current or

Table 4
Area statistics of disturbance detections based on ALOS-2 ScanSAR (L-Band) and Sentinel-1 data (C-Band) and the combined disturbance map.

Disturbance event sizes [ha]	**ALOS-2 ScanSAR**		**Sentinel-1**		**Combined**	
	Absolute area [kha]	Relative area [%]	Absolute area [kha]	Relative area [%]	Absolute area [kha]	Relative area [%]
<1	53.7	18.4	135.1	35.6	151.5	29.6
≥1 – <5	90.6	31.1	114.4	30.2	155.4	30.4
≥ 5	147.0	50.5	129.8	34.2	203.9	39.9
Total	291.3	100.0	379.3	100.0	510.8	100

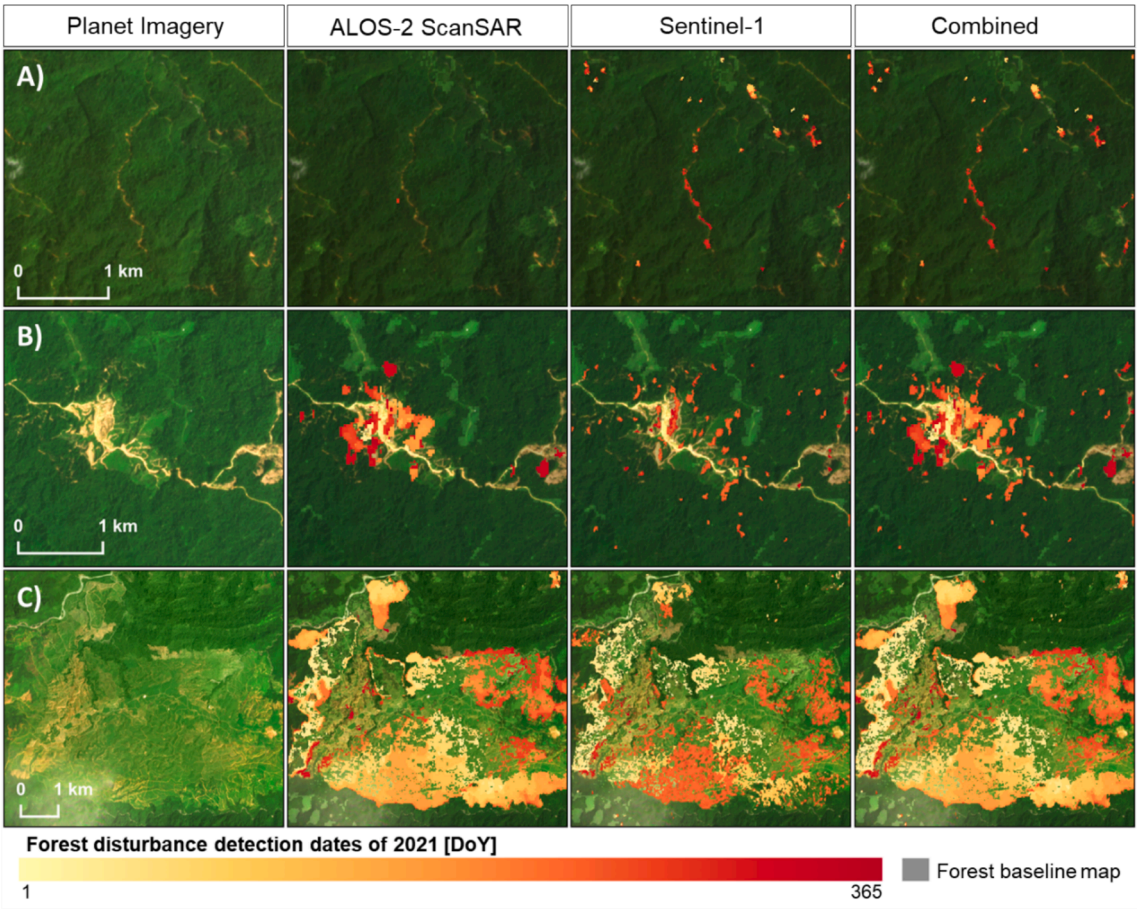

Fig. 3. Forest disturbance detection dates based on ALOS-2 ScanSAR (L-Band) and Sentinel-1 data (C-Band) and the combination of both disturbance detections for a small-(A), medium- (B) and large- (C) sized disturbance events. Post-disturbance monthly Planet imagery is provided as a basemap. Central coordinates for the events are: small-sized: 0.9176°S; 101.0301∘W; medium-sized: 4.426°N; 97.8016°W; large-sized: 4.9323°N; 97.0500°W.

Table 5
Mean temporal difference of detections [days] (standard deviation) relative to Sentinel-1 based detections. Positive values refer to a detection delay and negative values to improved detection timeliness. Values are based on disturbances detected in both ALOS-2 ScanSAR (L-Band) and Sentinel-1 data (C-Band). Areas are given for the overlapping disturbances detected in ALOS-2 ScanSAR and Sentinel-1 data.

Disturbance event sizes [ha]	**ALOS-2 ScanSAR**	**Combined**	Overlapping area [kha]
0.1 – <1	20.9 (80.2)	−20.2 (42.0)	8.2
≥1 – <5	25.1 (75.1)	−16.9 (37.9)	41.2
≥ 5	11.6 (62.9)	−17.0 (34.4)	112.1
Total	17.8 (68.6)	−16.5 (35.7)	161.5

older versions of the JJ-FAST product, to our ALOS-2 ScanSAR-based disturbance detections showed consistently higher producer accuracies of detections (1 ha: 50.6 ± 5.5 %; 1.5 ha: 46.9 ± 5.1 %; 2 ha: 45.1 ± 5 %) compared to the JJ-FAST product (29.2 ± 4.1 %).

A comparison of SAR-based disturbance maps from this study with 30 m operational Landsat-based products, GLAD-L alerts, and the annual GFC product showed similarly negligible commission errors (UA: 100 % ± 0) (Table 6). However, the optical-based forest disturbances had rather low producer accuracies (GLAD-L: 15.4 % ± 2.7 %; GFC: 54.3 % ± 7.6). The alerting system GLAD-L exhibited more omission errors than all SAR-based disturbance maps, while the annual GFC product showed more omission errors only when compared to the Sentinel-1 and the combined Sentinel-1 and ALOS-2 disturbance detections.

5. Discussion

We assessed the potential of medium resolution ALOS-2 PALSAR-2 ScanSAR data (100 m resolution) for tropical forest disturbance

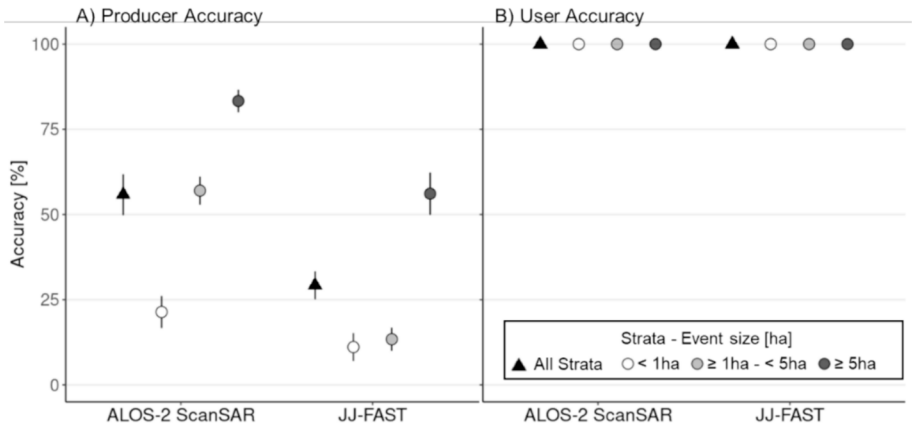

Fig. 4. Producer (A) and User (B) accuracies (±standard error) for all forest disturbances detected in our study and detected by JJ-FAST using ALOS-2 ScanSAR data. Accuracies are given for all strata (stable and disturbed forest) and only for the disturbance strata of small- (<1ha), medium- (>= 1 ha – < 5 ha), and large-sized disturbance events (>= 5 ha).

Table 6
Producer and User accuracy for SAR-based disturbance detections of this study and optical-based disturbance detections of the Global Forest change product for 2021.

	Producer accuracy ± standard error [%]	**User accuracy** ± standard error [%]
SAR-based (Our study)		
Sentinel-1	63.3 ± 9.6	100 ± 0
ALOS-PALSAR-2 ScanSAR	40.7 ± 6.3	98.6 ± 0.8
Combined	78.9 ± 11.9	99.3 ± 0.4
Optical-based (existing products)		
GLAD-L	15.4 ± 2.7	100 ± 0
GFC	54.3 ± 7.6	100 ± 0

mapping and demonstrated how the combination with high-resolution Sentinel-1 data (20 m resolution) can lead to more timely and accurate detections. Our findings further indicate that medium resolution ALOS-2 ScanSAR data is currently underutilized in the monitoring and alerting product JJ-FAST.

5.1. Potential of ALOS-2 ScanSAR data for tropical forest disturbance mapping

ALOS-2 ScanSAR data (L-Band) can reduce omission errors in Sentinel-1-based (C-Band) disturbance detections related to post-disturbance tree remnants in large-sized disturbance events (Fig. 5A). The backscatter values caused by post-disturbance tree remnants may resemble those of stable forest, reducing the contrast between stable and disturbed forest and hindering a disturbance detection. Although both short- (e.g., X-Band, C-Band) and long wavelength (e.g., L-Band) SAR data are affected (Balling et al., 2021; Watanabe et al., 2021), shorter wavelengths are more susceptible due to the radar signal's increased sensitivity in interacting with smaller objects (Balling et al., 2023). While incorporating texture, in addition to the individual pixel backscatter, was found to partially mitigate omission errors in disturbance detection based on short wavelengths (Balling et al., 2023), the introduction of false detections due to spatial blurring and increased computational costs presents a trade-off for its applicability on a large scale. Combining short- and long-wavelength SAR may offer a more viable path for large-scale applications. Moreover, we observed increased backscatter values for HH-polarized ALOS-2 ScanSAR data at locations with post-disturbance tree remnants (Fig. 5A). The increase of backscatter values in HH-polarization is typically related to amplified double bounce scattering on vertically oriented tree remnants (e.g., tree trunks) or enhanced direct scattering on horizontally oriented tree remnants (e.g., tree logs) (Watanabe et al., 2021). We utilized this characteristic to detect increased backscatter in HH-polarization as forest disturbances, leading to additional reductions in omission errors.

Medium resolution ALOS-2 ScanSAR data failed to detect many small-scale disturbances events, such as disturbance patches related to smallholder agriculture (Fig. 5B) or selective logging (Fig. 5C), that were detected by Sentinel-1 data (Doblas Prieto et al., 2023; Reiche et al., 2021). These omission errors are linked to the different spatial resolutions of ALOS-2 ScanSAR (~100 m) and Sentinel-1 (~20 m) and do not signify wavelength-specific detection advantages. The medium resolution of approximately 100 m of ALOS-2 ScanSAR data limit its detection capabilities to larger-sized events.

We observed higher detection rates of ALOS-2 ScanSAR-based disturbance detections for small- and medium-sized disturbance events when compared to detections of the JJ-FAST product, which can be likely related to the high minimum mapping unit of 2 ha applied in the JJ-FAST product tested (Version 3.0) (JICA and JAXA, 2023b). However, when applying coarser minimum mapping units (1 ha, 1.5 ha, or 2 ha) to our ALOS-2 ScanSAR-based disturbance detections, we consistently observed higher producer accuracies (1 ha: 50.6 %; 1.5 ha: 46.9 %; 2 ha: 45.1 %) than those achieved by the JJ-FAST product (29.2 %). This indicates that not only the coarse minimum mapping unit contribute to high omission errors in the JJ-FAST product, but potentially also the underlying detection method. This highlights the underutilized potential of the ALOS-2 ScanSAR data for large-scale operational monitoring. Newer versions of the JJ-FAST product apply a 1 ha minimum mapping unit and introduce improved detection methods (JICA and JAXA, 2023b), which might account for the high omission errors. However, these newer versions are not provided retrospectively (JICA and JAXA, 2023b).

5.2. Improvements in detection timeliness

The improved detection timeliness in the combined detections (up to 16.5 days), compared to detections relying solely on Sentinel-1 data, was primarily due to the capability of the long-wavelength ALOS-2 ScanSAR L-band data to detect forest disturbances characterized by post-disturbance tree remnants. Sentinel-1 shortwave C-band SAR is more prone to delayed detection at disturbance sites with tree remnants (Balling et al., 2023; Watanabe et al., 2021). Delayed detections arise when backscatter levels eventually decrease due to the removal of tree remnants, a process typically conducted for several land management practices.

Our results confirm that combining multi-sensor satellite data leads

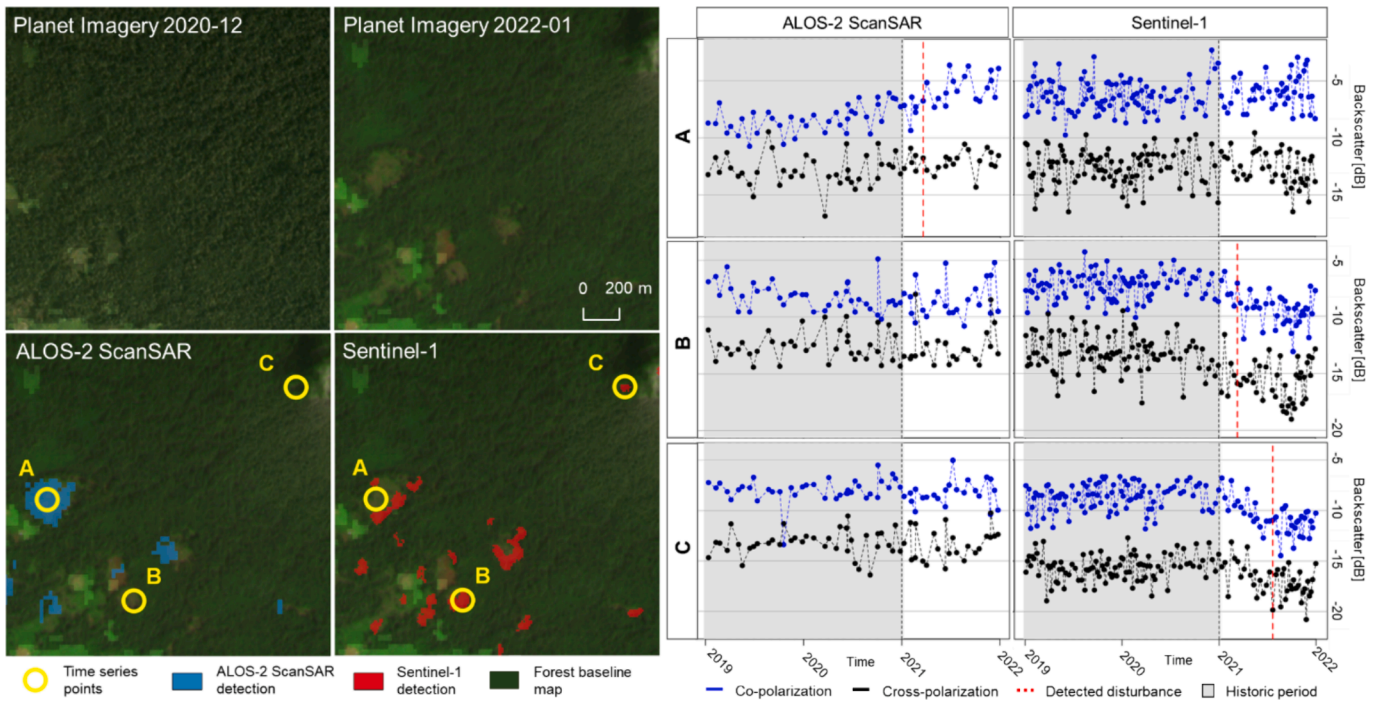

Fig. 5. Forest disturbances mapped using ALOS-2 ScanSAR (L-Band) or Sentinel-1 data (C-Band) in a region showing disturbance events attributed to or characterized by: tree remnants (A), smallholder agriculture (B), or selective logging (C). Backscatter time series from ALOS-2 ScanSAR (HH and HV) and Sentinel-1 data (VV and VH) are displayed in co- and cross-polarization, accompanied by the dates of detected disturbances. Additionally, pre-, and post-disturbance Planet imagery is provided.

to faster detections, corroborating previous studies (Chen et al., 2021; Reiche et al., 2018; Shimizu et al., 2019). Improved detection timeliness stems from increased observation density and the complementing ability to detect forest disturbances, including those with and without tree remnants and across scales from small to large.

5.3. *Current and future L-band missions for tropical forest disturbance detection*

Similar to previous studies, we would like to emphasize the necessity for a continuous data stream of freely available L-Band SAR data (Musthafa et al., 2021), in addition to the freely available C-Band data stream from Sentinel-1. Providing free access for ALOS-2 ScanSAR data also for other regions will accelerate the uptake of the data and enable improved large-scale forest monitoring.

Alongside ALOS-2, the SAOCOM mission has been providing L-Band data since 2018. However, freely accessible SAOCOM data is restricted to the European territory. Future acquisitions of L-Band SAR data over tropical forest environments are assured with three upcoming L-Band SAR missions, namely ALOS-4 PALSAR-3, NISAR, and ROSE-L (Motohka et al., 2019). The latter two missions will offer L-Band data free of charge, with spatial resolutions ranging from 3-50 m, and temporal resolution of up to 12 days (NISAR) and 6 days (ROSE-L) (ESA, 2023; NASA, n.d.), depending on the acquisition mode. The increased spatial resolution has the potential to overcome omission errors observed in this study for ALOS-2 ScanSAR-based disturbance detections, in particular concerning small-sized disturbance events.

5.4. *Comparison SAR-based and optical-based forest disturbance detection*

Comparing SAR-based disturbance detections of this study with optical Landsat-based disturbance products (e.g., GLAD-L & GFC) (Hansen et al., 2016, 2013) revealed omission errors in all of the single SAR-based and optical-based products. In particular, the optical-based alerting system GLAD-L exhibited severe omission errors (PA: 15.4 ± 2.7 %), which were much larger than those in all of the SAR-based detections (PA: Sentinel-1 63.3 ± 9.6 %; ALOS-2 ScanSAR 40.7 ± 6.3). SAR-based disturbance detections can outperform optical-based disturbance detections, especially in areas with persistent cloud cover (Doblas Prieto et al., 2023; Hirschmugl et al., 2020). However, in other regions, optical-based disturbance products can outperform SAR-based disturbance alerts (Doblas Prieto et al., 2023; Reiche et al., 2024) due to heightened sensor-specific omission errors in the SAR products, such as those caused by tree remnants (Balling et al., 2023, 2021; Watanabe et al., 2021).

Additionally, the accuracy of large-scale disturbance detection is closely linked to the dominant forest disturbance types, which have different effects on either SAR or optical remote sensing data. Reiche et al. (2024) provided a sophisticated comparison of SAR-based (RADD) and optical-based (GLAD-L & GLAD-S) disturbance monitoring and alerting systems for various forest disturbance types (e.g., large-scale clearings, selective logging, forest fires, etc.) and found that by integrating multi-sensor systems, it is possible to overcome sensor-specific omission errors and increase detection timeliness and confidence.

6. Conclusion

In this study, we mapped forest disturbances based on medium resolution ALOS-2 ScanSAR and high-resolution Sentinel-1 data and combined both disturbance detections. The combined forest disturbance detections exhibited substantially decreased omission errors, with minimum false detection rates, compared to single-sensor disturbance detections. Long wavelength ALOS-2 ScanSAR data (L-Band) has been shown to be particularly beneficial for detecting large-sized disturbance events characterized by post-disturbance tree remnants, which frequently cause omission errors or delayed detections for short wavelength SAR data like Sentinel-1C-Band. The medium spatial resolution of approximately 100 m limits the detection capability of ALOS-2 ScanSAR data to detect small-sized disturbances events (e.g., selective logging,

logging roads, etc.), that are correctly detected by Sentinel-1 data. Combining disturbance detections from both sensors resulted in an average improvement in detection timeliness of 16.5 days compared to using Sentinel-1 detections alone. Forest disturbance detections based on ALOS-2 ScanSAR data resulted in considerably higher detection rates when compared with the ALOS-2 ScanSAR data-based JJ-FAST alerting product. The high omission errors of the JJ-FAST product (Version 3.0) are linked to the coarse 2 ha minimum mapping unit, resulting in missed detections, especially for small- and medium-sized disturbance events. Comparing the SAR-based (C- and L-Band) disturbance detections from this study with existing optical-based forest disturbance products (GLAD-L and GFC) suggested improved detection accuracies when combining SAR and optical data. This improvement is achieved by overcoming sensor-specific omission errors, which is particularly beneficial in challenging environments such as tropical forests. Upcoming L-Band satellite missions, like NiSAR and ROSE-L, will offer freely accessible high-resolution L-Band SAR data, amplifying the potential demonstrated by L-Band ALOS-2 ScanSAR data. Our study highlights the necessity for freely available SAR data at C- and L-Band in order to accurately detect forest disturbances, in particular disturbance types associated with high temporal dynamics and complex structural properties.

CRediT authorship contribution statement

Johannes Balling: Writing – review & editing, Supervision, Methodology, Investigation, Funding acquisition, Conceptualization. **Bart Slagter:** Writing – review & editing, Validation, Methodology, Data curation. **Sietse van der Woude:** Writing – review & editing, Methodology, Data curation. **Martin Herold:** Writing – review & editing, Supervision, Funding acquisition, Conceptualization. **Johannes Reiche:** Writing – review & editing, Supervision, Methodology, Investigation, Funding acquisition, Conceptualization.

Declaration of competing interest

The authors declare that they have no known competing financial interests or personal relationships that could have appeared to influence the work reported in this paper.

Data availability

Data will be made available on request.

Acknowledgments

This study was funded by the USA Government's SilvaCarbon program, Norway's Climate and Forest Initiative (NICFI), by the Open-Earth-Monitor Cyberinfrastructure project (grant agreement No. 101059548), by the ForestWard Observatory to Secure Resilience of European Forests (FORWARDS) project (grant agreement No. 101084481) and by the Open Domain Science project Forest Carbon Crime (Project Number: OCENW.M.21.203) of the Nederlandse Organisatie voor Wetenschappelijk Onderzoek (NWO). This research involves modified ALOS-2 PALSAR-2 ScanSAR data provided by Earth Observation Research Center (EORC) of Japan Aerospace Exploration Agency (JAXA) and Copernicus Sentinel-1 data (2018-2021). Planet imagery was accessed through the NICFI program.

We would like to thank Nandika Tsendbazar and Maciej Soja for their help conducting this study.

We thank the two anonymous reviewers for their valuable feedback and comments, which greatly improved the quality of the manuscript.

References

Abood, S.A., Lee, J.S.H., Burivalova, Z., Garcia-Ulloa, J., Koh, L.P., 2015. Relative Contributions of the Logging, Fiber, Oil Palm, and Mining Industries to Forest Loss in Indonesia. Conserv. Lett. 8, 58–67. https://doi.org/10.1111/conl.12103.

Ali, M.Z., Qazi, W., Aslam, N., 2018. A comparative study of ALOS-2 PALSAR and landsat-8 imagery for land cover classification using maximum likelihood classifier. Egypt. J. Remote Sens. Space Sci. 21, S29–S35. https://doi.org/10.1016/j.ejrs.2018.03.003.

Austin, K.G., Schwantes, A., Gu, Y., Kasibhatla, P.S., 2019. What causes deforestation in Indonesia? Environ. Res. Lett. 14, 024007 https://doi.org/10.1088/1748-9326/aaf6db.

Ballère, M., Bouvet, A., Mermoz, S., Le Toan, T., Koleck, T., Bedeau, C., André, M., Forestier, E., Frison, P.-L., Lardeux, C., 2021. SAR data for tropical forest disturbance alerts in French Guiana: Benefit over optical imagery. Remote Sens. Environ. 252, 112159 https://doi.org/10.1016/j.rse.2020.112159.

Balling, J., Verbesselt, J., De Sy, V., Herold, M., Reiche, J., 2021. Exploring archetypes of tropical fire-related forest disturbances based on dense optical and radar satellite data and active fire alerts. Forests 12, 456. https://doi.org/10.3390/f12040456.

Balling, J., Herold, M., Reiche, J., 2023. How textural features can improve SAR-based tropical forest disturbance mapping. Int. J. Appl. Earth Obs. Geoinf. 124, 103492 https://doi.org/10.1016/j.jag.2023.103492.

Boulton, C.A., Lenton, T.M., Boers, N., 2022. Pronounced loss of Amazon rainforest resilience since the early 2000s. Nat. Clim. Chang. 12 https://doi.org/10.1038/s41558-022-01287-8.

Chen, N., Tsendbazar, N.-E., Hamunyela, E., Verbesselt, J., Herold, M., 2021. Sub-annual tropical forest disturbance monitoring using harmonized Landsat and Sentinel-2 data. Int. J. Appl. Earth Obs. Geoinf. 102, 102386 https://doi.org/10.1016/j.jag.2021.102386.

Danklmayer, A., Doring, B.J., Schwerdt, M., Chandra, M., 2009. Assessment of atmospheric propagation effects in SAR images. IEEE Trans. Geosci. Remote Sens. 47, 3507–3518. https://doi.org/10.1109/TGRS.2009.2022271.

De Sy, V., Herold, M., Achard, F., Asner, G.P., Held, A., Kellndorfer, J., Verbesselt, J., 2012. Synergies of multiple remote sensing data sources for REDD+ monitoring. Curr. Opin. Environ. Sustain. 4, 696–706. https://doi.org/10.1016/j.cosust.2012.09.013.

Doblas, J., Carneiro, A., Shimabukuro, Y., Sant'Anna, S., Aragao, L., 2020. Assessment of rainfall influence on sentinel-1 time series on Amazonian tropical forests aiming deforestation detection improvement. In: 2020 IEEE Latin American GRSS & ISPRS Remote Sensing Conference (LAGIRS). IEEE, pp. 397–402. https://doi.org/10.1109/LAGIRS48042.2020.9165566.

Doblas Prieto, J., Lima, L., Mermoz, S., Bouvet, A., Reiche, J., Watanabe, M., Sant Anna, S., Shimabukuro, Y., 2023. Inter-comparison of optical and SAR-based forest disturbance warning systems in the Amazon shows the potential of combined SAR-optical monitoring. Int. J. Remote Sens. 44, 59–77. https://doi.org/10.1080/01431161.2022.2157684.

Doblas, J., Reis, M.S., Belluzzo, A.P., Quadros, C.B., Moraes, D.R.V., Almeida, C.A., Maurano, L.E.P., Carvalho, A.F.A., Sant'Anna, S.J.S., Shimabukuro, Y.E., 2022. DETER-R: An operational near-real time tropical forest disturbance warning system based on Sentinel-1 time series analysis. Remote Sens. (Basel) 14, 3658. https://doi.org/10.3390/rs14153658.

ESA, 2012. Sentinel-1: ESA's Radar Observatory Mission for GMES Operational Services, ESA Special Publication. ESA Communications, Noordwijk, The Netherlands.

ESA, 2022. Sentinel-1 Observation Scenario [WWW Document]. URL https://sentinels.copernicus.eu/web/sentinel/missions/sentinel-1/observation-scenario (accessed 7.19.22).

ESA, 2023. ROSE-L (Radar Observing System for Europe in L-band) [WWW Document]. URL https://www.eoportal.org/satellite-missions/rose-l-radar-observing-system-for-europe-in-l-band-#eop-quick-facts-section (accessed 10.1.23).

ESA, n.d. About SAOCOM [WWW Document]. URL https://earth.esa.int/eogateway/missions/saocom (accessed 10.1.23).

Finer, M., Novoa, S., Weisse, M.J., Petersen, R., Mascaro, J., Souto, T., Stearns, F., Martinez, R.G., 2018. Combating deforestation: From satellite to intervention. Science 1979 (360), 1303–1305. https://doi.org/10.1126/science.aat1203.

Flores-Anderson, A.I., Herndon, K.E., Thapa, R.B., Cherrington, E., 2019. The SAR Handbook: Comprehensive Methodologies for Forest Monitoring and Biomass Estimation. SERVIR, Huntsvile.

Gaveau, D.L.A., Sloan, S., Molidena, E., Yaen, H., Sheil, D., Abram, N.K., Ancrenaz, M., Nasi, R., Quinones, M., Wielaard, N., Meijaard, E., 2014. Four decades of forest persistence, clearance and logging on Borneo. PLoS One 9, 1–11. https://doi.org/10.1371/journal.pone.0101654.

Google Earth Engine Team, 2022. Sentinel-1 Algorithms: Pre-processing [WWW Document]. URL https://developers.google.com/earth-engine/guides/sentinel1 (accessed 7.12.22).

Gumbricht, T., Román-Cuesta, R.M., Verchot, L.V., Herold, M., Wittmann, F., Householder, E., Herold, N., Murdiyarso, D., 2017. Tropical and Subtropical Wetlands Distribution.

Hamunyela, E., Verbesselt, J., Herold, M., 2016. Using spatial context to improve early detection of deforestation from Landsat time series. Remote Sens. Environ. 172, 126–138. https://doi.org/10.1016/j.rse.2015.11.006.

Hansen, M.C., Potapov, P.V., Moore, R., Hancher, M., Turubanova, S.A., Tyukavina, A., Thau, D., Stehman, S.V., Goetz, S.J., Loveland, T.R., Kommareddy, A., Egorov, A., Chini, L., Justice, C.O., Townshend, J.R.G., 2013. High-resolution global maps of 21st-century forest cover change. Science 1979 (342), 850–853. https://doi.org/10.1126/science.1244693.

Hansen, M.C., Krylov, A., Tyukavina, A., Potapov, P.V., Turubanova, S., Zutta, B., Ifo, S., Margono, B., Stolle, F., Moore, R., 2016. Humid tropical forest disturbance alerts using Landsat data. Environ. Res. Lett. 11, 034008 https://doi.org/10.1088/1748-9326/11/3/034008.

Hayasaka, H., 2023. Peatland fire weather conditions in Sumatra, Indonesia. Climate 11, 92. https://doi.org/10.3390/cli11050092.

Hirschmugl, M., Deutscher, J., Sobe, C., Bouvet, A., Mermoz, S., Schardt, M., 2020. Use of SAR and optical time series for tropical forest disturbance mapping. Remote Sens. (Basel) 12, 727. https://doi.org/10.3390/rs12040727.

Hoekman, D.H., Reiche, J., 2015. Multi-model radiometric slope correction of SAR images of complex terrain using a two-stage semi-empirical approach. Remote Sens. Environ. 156, 1–10. https://doi.org/10.1016/j.rse.2014.08.037.

JAXA, 2023. ALOS-2 PALSAR-2 ScanSAR Products [WWW Document]. URL https://www.eorc.jaxa.jp/ALOS/en/dataset/palsar2_l22_e.htm (accessed 9.24.23).

JAXA, n.d. PALSAR-2 [WWW Document]. URL https://www.eorc.jaxa.jp/ALOS/en/alos-2/a2_sensor_e.htm (accessed 10.1.23).

JICA & JAXA, 2023. JJ-Fast MapMonitor [WWW Document]. URL https://www.eorc.jaxa.jp/jjfast/jj_mapmonitor_phase1.html (accessed 10.4.23).

JICA, JAXA, 2023a. JJ-FAST Technical Note (Ver. 8).

JICA, JAXA, 2023b. JJ-FAST Technical Note. Version 9.1.

JICA, JAXA, 2024. JJ-FAST technical note [WWW Document]. URL https://www.eorc.jaxa.jp/jjfast/note.html (accessed 5.17.24).

Joshi, N., Baumann, M., Ehammer, A., Fensholt, R., Grogan, K., Hostert, P., Jepsen, M.R., Kuemmerle, T., Meyfroidt, P., Mitchard, E.T.A., Reiche, J., Ryan, C.M., Waske, B., 2016. A review of the application of optical and radar remote sensing data fusion to land use mapping and Monitoring. Remote Sens. (Basel) 8. https://doi.org/10.3390/rs8010070.

Liang, C., Fielding, E.J., 2017. Interferometry with ALOS-2 full-aperture ScanSAR data. IEEE Trans. Geosci. Remote Sens. 55, 2739–2750. https://doi.org/10.1109/TGRS.2017.2653190.

Margono, B.A., Turubanova, S., Zhuravleva, I., Potapov, P., Tyukavina, A., Baccini, A., Goetz, S., Hansen, M.C., 2012. Mapping and monitoring deforestation and forest degradation in Sumatra (Indonesia) using Landsat time series data sets from 1990 to 2010. Environ. Res. Lett. 7 https://doi.org/10.1088/1748-9326/7/3/034010.

Margono, B.A., Potapov, P.V., Turubanova, S., Stolle, F., Hansen, M.C., 2014. Primary forest cover loss in Indonesia over 2000–2012. Nat. Clim. Chang. 4, 730–735. https://doi.org/10.1038/nclimate2277.

Mermoz, S., Bouvet, A., Koleck, T., Ballère, M., Le Toan, T., 2021. Continuous detection of forest loss in Vietnam, Laos, and Cambodia using Sentinel-1 data. Remote Sens. (Basel) 13, 4877. https://doi.org/10.3390/rs13234877.

Motohka, T., Kankaku, Y., Miura, S., Suzuki, S., 2019. Alos-4 L-band SAR mission and observation. In: IGARSS 2019–2019 IEEE International Geoscience and Remote Sensing Symposium. IEEE, pp. 5271–5273. https://doi.org/10.1109/IGARSS.2019.8898169.

Mullissa, A., Vollrath, A., Odongo-Braun, C., Slagter, B., Balling, J., Gou, Y., Gorelick, N., Reiche, J., 2021. Sentinel-1 SAR Backscatter analysis ready data preparation in Google Earth engine. Remote Sens. (Basel) 13, 1954. https://doi.org/10.3390/rs13101954.

Musthafa, M., Singh, G., Nela, B.R., 2021. Time-series analysis of C-band and L-band Sar Backscatter in detecting forest disturbance and regrowth dynamics. In: 2021 IEEE International India Geoscience and Remote Sensing Symposium (InGARSS). IEEE, pp. 10–13. https://doi.org/10.1109/InGARSS51564.2021.9792018.

NASA, n.d. NISAR: Quick Facts [WWW Document]. URL https://nisar.jpl.nasa.gov/mission/quick-facts/ (accessed 10.1.23).

Natsuaki, R., Nagai, H., Motohka, T., Ohki, M., Watanabe, M., Thapa, R.B., Tadono, T., Shimada, M., Suzuki, S., 2016. SAR interferometry using ALOS-2 PALSAR-2 data for the Mw 7.8 Gorkha, Nepal earthquake. Earth Planets Space 68, 15. https://doi.org/10.1186/s40623-016-0394-4.

Olofsson, P., Foody, G.M., Herold, M., Stehman, S.V., Woodcock, C.E., Wulder, M.A., 2014. Good practices for estimating area and assessing accuracy of land change. Remote Sens. Environ. 148, 42–57. https://doi.org/10.1016/j.rse.2014.02.015.

Olofsson, P., Arévalo, P., Espejo, A.B., Green, C., Lindquist, E., McRoberts, R.E., Sanz, M. J., 2020. Mitigating the effects of omission errors on area and area change estimates. Remote Sens. Environ. 236, 111492 https://doi.org/10.1016/j.rse.2019.111492.

Planet Team, 2022. Planet Application Program Interface: In Space for Life on Earth Online [WWW Document]. URL https://api.planet.com (accessed 7.12.22).

Quegan, S., Yu, J.J., 2001. Filtering of multichannel SAR images. IEEE Trans. Geosci. Remote Sens. 39, 2373–2379. https://doi.org/10.1109/36.964973.

Refice, A., Zingaro, M., D'Addabbo, A., Chini, M., 2020. Integrating C- and L-band SAR imagery for detailed flood monitoring of remote vegetated areas. Water (Basel) 12, 2745. https://doi.org/10.3390/w12102745.

Reiche, J., de Bruin, S., Hoekman, D., Verbesselt, J., Herold, M., 2015. A Bayesian approach to combine landsat and ALOS PALSAR time series for near real-time deforestation detection. Remote Sens. (Basel) 7, 4973–4996. https://doi.org/10.3390/rs70504973.

Reiche, J., Hamunyela, E., Verbesselt, J., Hoekman, D., Herold, M., 2018. Improving near-real time deforestation monitoring in tropical dry forests by combining dense Sentinel-1 time series with Landsat and ALOS-2 PALSAR-2. Remote Sens. Environ. 204, 147–161. https://doi.org/10.1016/j.rse.2017.10.034.

Reiche, J., Mullissa, A., Slagter, B., Gou, Y., Tsendbazar, N.-E., Odongo-Braun, C., Vollrath, A., Weisse, M.J., Stolle, F., Pickens, A., Donchyts, G., Clinton, N., Gorelick, N., Herold, M., 2021. Forest disturbance alerts for the Congo Basin using Sentinel-1. Environ. Res. Lett. 16, 024005 https://doi.org/10.1088/1748-9326/abd0a8.

Reiche, J., Balling, J., Pickens, A.H., Masolele, R.N., Berger, A., Weisse, M.J., Mannarino, D., Gou, Y., Slagter, B., Donchyts, G., Carter, S., 2024. Integrating satellite-based forest disturbance alerts improves detection timeliness and confidence. Environ. Res. Lett. 19, 054011 https://doi.org/10.1088/1748-9326/ad2d82.

Richards, J.A., 2009. Remote Sensing with Imaging Radar. Springer, Berlin Heidelberg, Berlin, Heidelberg https://doi.org/10.1007/978-3-642-02020-9.

Saputra, M.H., Lee, H.S., 2019. Prediction of land use and land cover changes for North Sumatra, Indonesia, using an artificial-neural-network-based cellular automaton. Sustainability 11, 3024. https://doi.org/10.3390/su11113024.

Shimizu, K., Ota, T., Mizoue, N., 2019. Detecting forest changes using dense Landsat 8 and Sentinel-1 time series data in tropical seasonal forests. Remote Sens. (Basel) 11, 1899. https://doi.org/10.3390/rs11161899.

Singh, M., Yan, S., 2021. Spatial–temporal variations in deforestation hotspots in Sumatra and Kalimantan from 2001–2018. Ecol. Evol. 11, 7302–7314. https://doi.org/10.1002/ece3.7562.

Sloan, S., Locatelli, B., Wooster, M.J., Gaveau, D.L.A., 2017. Fire activity in Borneo driven by industrial land conversion and drought during El Niño periods, 1982–2010. Glob. Environ. Chang. 47, 95–109. https://doi.org/10.1016/j.gloenvcha.2017.10.001.

Small, D., 2011. Flattening gamma: Radiometric terrain correction for SAR imagery. IEEE Trans. Geosci. Remote Sens. 49, 3081–3093. https://doi.org/10.1109/TGRS.2011.2120616.

Stehman, S.V., 2014. Estimating area and map accuracy for stratified random sampling when the strata are different from the map classes. Int. J. Remote Sens. 35, 4923–4939. https://doi.org/10.1080/01431161.2014.930207.

Stehman, S.V., Wickham, J.D., Smith, J.H., Yang, L., 2003. Thematic accuracy of the 1992 National Land-Cover Data for the eastern United States: Statistical methodology and regional results. Remote Sens. Environ. 86, 500–516. https://doi.org/10.1016/S0034-4257(03)00128-7.

Sullivan, M.J.P., Talbot, J., Lewis, S.L., Phillips, O.L., Qie, L., Begne, S.K., Chave, J., Cuni-sanchez, A., Hubau, W., Lopez-, G., Miles, L., Monteagudo-mendoza, A., Sonké, B., Doucet, J., Erwin, T.L., Espejo, J.S., Ewango, C.E.N., 2017. Diversity and carbon storage across the tropical forest biome. Sci. Rep. 1–12 https://doi.org/10.1038/srep39102.

Tabor, K.M., Holland, M.B., 2021. Opportunities for improving conservation early warning and alert systems. Remote Sens. Ecol. Conserv. 7, 7–17. https://doi.org/10.1002/rse2.163.

Tsendbazar, N., Herold, M., Li, L., Tarko, A., de Bruin, S., Masiliunas, D., Lesiv, M., Fritz, S., Buchhorn, M., Smets, B., Van De Kerchove, R., Duerauer, M., 2021. Towards operational validation of annual global land cover maps. Remote Sens. Environ. 266, 112686 https://doi.org/10.1016/j.rse.2021.112686.

Ulaby, F., Long, D., 2013. Microwave Radar and Radiometric Remote Sensing, unabridged. ed. The University of Michigan Press.

Urbazaev, M., Cremer, F., Migliavacca, M., Reichstein, M., Schmullius, C., Thiel, C., 2018. Potential of multi-temporal ALOS-2 PALSAR-2 ScanSAR data for vegetation height estimation in tropical forests of Mexico. Remote Sens. (Basel) 10, 1277. https://doi.org/10.3390/rs10081277.

Valeriano, D.M., Amaral, S., 2010. K&C Science Report - Phase 1 Application of ALOS/PALSAR in support to Brazilian Forest Monitoring Program.

Vancutsem, C., Achard, F., Pekel, J.-F., Vieilledent, G., Carboni, S., Simonetti, D., Gallego, J., Aragão, L.E.O.C., Nasi, R., 2021. Long-term (1990–2019) monitoring of forest cover changes in the humid tropics. Sci. Adv. 7 https://doi.org/10.1126/sciadv.abe1603.

Vargas, C., Montalban, J., Leon, A.A., 2019. Early warning tropical forest loss alerts in Peru using Landsat. Environ Res Commun 1, 121002. https://doi.org/10.1088/2515-7620/ab4ec3.

Verbesselt, J., Zeileis, A., Herold, M., 2012. Near real-time disturbance detection using satellite image time series. Remote Sens. Environ. 123, 98–108. https://doi.org/10.1016/j.rse.2012.02.022.

Verhelst, K., Gou, Y., Herold, M., Reiche, J., 2021. Improving forest baseline maps in tropical wetlands using GEDI-based forest height information and Sentinel-1. Forests 12, 1374. https://doi.org/10.3390/f12101374.

Vollrath, A., Mullissa, A., Reiche, J., 2020. Angular-based radiometric slope correction for Sentinel-1 on Google Earth engine. Remote Sens. (Basel) 12, 1867. https://doi.org/10.3390/rs12111867.

Watanabe, M., Koyama, C.N., Hayashi, M., Nagatani, I., Shimada, M., 2018. Early-stage deforestation detection in the tropics With *L*-band SAR. IEEE J. Sel. Top. Appl. Earth Obs. Remote Sens. 11, 2127–2133. https://doi.org/10.1109/JSTARS.2018.2810857.

Watanabe, M., Koyama, C.N., Hayashi, M., Nagatani, I., Tadono, T., Shimada, M., 2021. Refined algorithm for forest early warning system with ALOS-2/PALSAR-2 ScanSAR data in tropical forest regions. Remote Sens. Environ. 265, 112643 https://doi.org/10.1016/j.rse.2021.112643.

Whittle, M., Quegan, S., Uryu, Y., Stüewe, M., Yulianto, K., 2012. Detection of tropical deforestation using ALOS-PALSAR: A Sumatran case study. Remote Sens. Environ. 124, 83–98. https://doi.org/10.1016/j.rse.2012.04.027.

Woodhouse, I.H., 2006. Introduction to Microwave Remote Sensing, 1st ed. CRC Press.